A THERMALIZED ION EXPLOSION MODEL FOR HIGH ENERGY SPUTTERING AND TRACK REGISTRATION

Thesis by

Lucy Elizabeth Seiberling

In Partial Fulfillment of the Requirements

for the Degree of

Doctor of Philosophy

California Institute of Technology

Pasadena, California

1980

(Submitted May 21, 1980)

ACKNOWLEDGMENTS

The results and ideas presented in this thesis evolved from the work of many before me. Most notably, Tom Tombrello motivated, directed and obtained financial support for the continuing endeavor. No less important was the moral support and encouragement he provided in times of slow progress. Others whose contributions were crucial to this work are: Joe Griffith, Pete Haff, Bob Weller and Don Burnett. In addition to his pioneering work on high energy sputtering, Joe Griffith motivated the effort to see charged clusters sputtered from UF_4. He also generously gave many hours of his time during the execution of the experiment. Steve Koonin and Charles Watson also made fruitful comments and suggestions.

I would also like to acknowledge the many competent and cheerful members of the secretarial and technical staff. Special mention goes to Wil Schick whose talent, insight and patience will always endear him to me.

Finally, I wish to thank Bill for sharing with me his warmth and humor.

This thesis is dedicated to the memory of my parents.

ABSTRACT

A velocity spectrum of neutral sputtered particles as well as a low resolution mass spectrum of sputtered molecular ions has been measured for 4.74 MeV $^{19}F^{+2}$ incident on UF_4. The velocity spectrum is dramatically different from spectra taken with low energy (keV) bombarding ions, and is shown to be consistent with a hot plasma of atoms in thermal equilibrium inside the target. We propose a "thermalized ion explosion" model for high energy sputtering which is also expected to describe track formation in dielectric materials. The model is shown to be consistent with the observed total sputtering yield and the dependence of the yield on the primary ionization rate of the incident ion.

TABLE OF CONTENTS

I. INTRODUCTION

Two independent but almost simultaneous developments in Kellogg led to an association between high energy sputtering and track formation in dielectric materials. By high energy sputtering we mean sputtering associated with the electronic stopping power of the bombarding ion. The first was a prediction by Haff (1976) that the process of track formation in dielectric solids could lead to an enhancement of the sputtering of the target material, and the second was the development by Gregg, Switkowski and Tombrello (1977) of a very sensitive technique for measuring sputtered uranium using solid state track detectors. The prediction by Haff was based on the ion explosion model of track formation proposed by Fleischer et al. (1965). In this model, adjacent target atoms which are ionized by the passing beam particle repel each other due to Coulomb forces. The recoiling ions strike neighboring atoms and set up a weak collision cascade or lodge in interstitial sites. The resulting damage to the crystal lattice, which extends radially about 30 ± 15 Å from the ion path (Fleischer et al. 1975), is known as the latent track. Haff suggested that the weak collision cascades would lead to sputtered particles in much the same way that collision cascades lead to sputtering with low energy ion bombardment (Sigmund 1969).

Another model for track formation is the thermal spike model due to Chadderton et al. (1966). In this model, electrons scattered by the impinging ion repeatedly collide with target atoms, thereby transferring heat into the lattice and causing a localized region around the ion path to melt. Both models are in qualitative agreement with existing track

registration data, and it is unlikely that track registration data alone will be able to determine the correct model. It should be noted here that the thermal spike model of track formation would also be expected to lead to sputtered particles, i.e. particles which evaporate from the hot surface. The velocity distribution of these particles would be thermal in nature and should be quite distinct from the velocity distribution due to a (non-thermal) weak collision cascade.

Conventional (low energy) sputtering theory (Sigmund 1969) predicts very small yields ($\lesssim 10^{-3}$) for ions in the electronic stopping region, where track formation is important. For this reason, the enhanced yields (of order unity) associated with track formation would be very easy to detect. The promise of discovering a new sputtering mechanism, and of using the sputtered particles to understand track registration led to several important experiments which were performed in Kellogg. The first was the demonstration that high energy, heavy ions indeed produce large sputtering yields in uranium tetrafluoride, a crystalline dielectric solid. This work was performed by J. E. Griffith (1979). He discovered yields as much as three orders of magnitude higher than predicted by Sigmund theory. Investigators in other laboratories have independently discovered other dielectric materials which exhibit enhanced sputtering with high energy ions; for example, Brown et al. (1980) with frozen H_2O targets, and Ollerhead et al. (1980) with frozen xenon. Another important step was the development of a mechanical time of flight (TOF) spectrometer which was capable of measuring the velocity spectrum of the sputtered uranium particles. The design and construction of such a spectrometer, as well as the demonstration of its use with sputtered particles from low energy ion

bombardment, was the subject of the thesis by R. A. Weller (1978).

At this point, two attempts were made to determine the TOF spectrum of uranium sputtered from UF_4 by 4.74 MeV $^{19}F^{+2}$ ions. The first spectrum, displayed in Griffith (1979) Figure 34, revealed two things: a substantial fraction of the sputtered particles are charged, and in general the particles have very low energy (< 1 eV). These were unexpected properties in terms of ordinary sputtering and required modifications to the experiment, after which another spectrum was taken. The second spectrum is shown in Figure 1, taken from Griffith's thesis (1979). During this run, the target, as well as all surfaces along the sputtered particle flight path, were at ground potential. In principle, the TOF spectrum contains charged as well as neutral particles; however, most of the sputtered ions (which leave the target with a few eV or less) are probably bent from the flight path by ambient magnetic fields. Therefore, it is likely that Figure 1 is a TOF spectrum of neutral particles only. The TOF data are plotted in Griffith (1979) as an energy spectrum and analysed in terms of a collisional and a thermal model of sputtering. It is not clear from this analysis which model best describes the sputtering process.

In this thesis, two additional TOF spectra will be presented. The first was taken with 80 keV $^{20}Ne^{+}$ on UF_4 in order to demonstrate that UF_4 obeys Sigmund sputtering theory under low energy ion bombardment. The second was again taken with 4.74 MeV $^{19}F^{+2}$. In this run, the target was biased at +100 volts, thereby separating the sputtered ions from the neutrals in a controlled manner. The resolution of the spectrometer was improved, which permitted the separation of charged clusters differing in mass by about 200 amu. The neutral part of this spectrum, upon which the

model in this thesis is based, is not significantly different from the spectrum shown in Figure 1. The difference here is in the analysis and interpretation of the data.

II. THE EXPERIMENTS

A. APPARATUS AND HARDWARE

A schematic drawing of the TOF spectrometer developed by Weller and Tombrello (1978) is shown in Figure 2. An ion beam enters the motor chamber and is chopped by a slit in a rotating wheel. The beam pulse travels through a fixed slit and strikes a target surface approximately 75 cm from the wheel. Particles which are sputtered normal to the surface travel back along the beam line, are collimated by the fixed slit, and land on the rotating wheel. After the sputtered particles are collected, a freshly cleaved piece of mica is placed against the wheel, and the resulting layered package is exposed to a flux of thermal neutrons. The ^{235}U is then detected by observing neutron induced fission fragment tracks in the mica. This technique for detecting sputtered uranium is described by Gregg (1977). A complete description of the design and operation of the spectrometer can be found in the thesis by R. A. Weller (1978).

The low energy run was performed on the sputtering beam line of the 150 kV duoplasmatron ion source. A positive ion beam is produced, which is momentum analysed by a 31° magnet before entering the motor chamber. The high energy run was performed on the north 10° beam line of the Caltech tandem accelerator. A 90° magnet is used to momentum select the positive ion beam. An in-line cold trap separates the motor chamber (at a pressure of $\sim 1 \times 10^{-6}$ torr) from the UHV chamber which contains the target (at $\sim 1 \times 10^{-8}$ torr). The target for both runs consisted of an evaporated UF_4 film approximately 5000 Å thick on a polished copper backing, as described further in Griffith (1979), section III. E. 5.

Several modifications of the spectrometer were made for the high energy experiment and they will be described in part B of this section. The most important change pertains to the resolution of the spectrometer. The factors which determine the resolution are simple to understand, yet easy to overlook, and we feel that a short digression on this topic is warranted here. In principle, three factors limit the resolution of our data analysis technique. Two are related to data collection and one to track counting. These factors are the stability of the motor revolution rate, the finite width of the fixed and moving slits, and the width of the band on which tracks are counted for a given data point. The motor period is monitored during the run and is stable to less than 0.1 μsec. The width of the microscope field of view used in counting tracks is 200 μm, which corresponds to a range in TOF of 1.3 μsec. In contrast to these relatively small times, the slit width corresponds to 28 μsec. That is, it takes 28 μsec for the moving slit to pass a fixed point.

How does a given slit width relate to resolution in TOF? (We consider both the fixed and moving slits to have the same width.) Since the moving slit is used to chop the beam, a square pulse of length 28 μsec will result if the beam is well focused. Consider only particles which sputter from the target with velocity v_o, corresponding to a TOF t_o. The pulse of sputtered particles will also have a length of 28 μsec, and the center of this pulse will arrive at the wheel after a time t_o. Now, the fixed slit collimates the sputtered particle pulse to a width which corresponds to a range of 28 μsec in TOF. At each point in time, particles are deposited in a band 28 μsec wide on the wheel and the deposition takes place uniformly for a time of 28 μsec. The superposition of both effects results in a tri-

angular distribution of particles along the wheel. The peak of the triangle is at time t_o and the full width at half maximum (FWHM) is 28 μsec. The slit width is clearly the dominant factor in determining the resolution of the spectrometer. It is also clear that two peaks must be at least one slit width apart on the wheel in order to be resolved. Decreasing the slit width, of course, decreases the rate at which particles are collected and necessitates an increase in the run time.

One additional factor should be mentioned before leaving the subject of resolution. We have shown above that the resolution in TOF depends primarily on the slit width and is not a function of t_o. In other words, for any t_o the FWHM of the particle distribution is $\pm$ 28 μsec. The energy resolution, however, is strongly dependent on t_o. This can be seen by the following simple argument: differentiating

$$\mathcal{E}_o = \tfrac{1}{2} M(L/t_o)^2 \qquad \text{gives}$$

$$|\Delta \mathcal{E}_o| = ML^2(\Delta t_o/t_o^3),$$

where $\mathcal{E}_o$ is the energy of a sputtered particle with TOF t_o (L is the target-collector distance). Since Δt_o is a constant,

$$\Delta \mathcal{E}_o \propto 1/t_o^3 \quad .$$

This implies that the range of energies which fall into a given band on the wheel of width Δt_o increases as $1/t_o^3$ for small TOF. Therefore, the energy resolution is much better at long times of flight (low energy) than at short times of flight (high energy).

B. PROCEDURE AND DATA ANALYSIS

The low energy run was performed with an 80 keV $^{20}Ne^{+}$ beam from the 150 kV duoplasmatron ion source. The average DC beam current on the target (after chopping) was kept between 0.5 and 1.5 μA. A spectrometer wheel 5.08 cm in radius with one slit, measuring 1.11 cm by 0.45 cm, was fabricated from 99.99% pure aluminum sheet 0.05 cm thick. The wheel rotated at 500 Hz, which gave a resolution in TOF of 28 μsec (FWHM). The target was kept at a temperature of 106°C during the run and the UHV chamber was at a pressure below 2×10^{-8} torr. It has been shown (Griffith 1979) that a clean surface is maintained on the UF_4 film by applying heat to the target prior to and during the run. All surfaces exposed to the sputtered particles, as well as the target, were at ground potential. The target was moved approximately 3 mm every two hours, limiting the beam fluence on any spot of the film to less than $8 \times 10^{16}/cm^2$. This run, shown in Figure 3, lasted about 27 hours.

The dramatic difference in the TOF spectra for high energy and low energy sputtering can be seen by comparing Figures 1 and 3. The unusual shape of the high energy spectrum has made it possible to accelerate the sputtered ions with a target bias, and collect them in a region where the neutral yield is very low. It was also possible to improve the resolution of our spectrometer sufficiently to resolve UF_n^+ molecules from $(UF_n)_2^+$ and $(UF_n)_3^+$ clusters (n is a small positive integer). A single slit of width 0.23 cm was chosen, which allowed peaks greater than 14 μsec apart to be resolved. This necessitated an increase in the run time to 45 hours. A target bias of +100 volts was used as a compromise between particle rigidity and resolution. A larger voltage would have decreased the TOF and

hence reduced the resolution (see discussion in section II. A.) while a smaller voltage would not have given the ions sufficient rigidity to withstand small magnetic fields along the flight path. Magnetic shielding was used to reduce ambient magnetic fields to less than 0.1 Gauss.

A grounded steel disc with a circular aperture was placed 4 cm in front of the target to form a ground plane. The ions were assumed to accelerate uniformly to 100 eV in 4 cm before drifting the remaining distance (71 cm) to the collector wheel. In calculating the TOF, the initial velocity of the sputtered ions was neglected. The high energy run was performed with a 4.74 MeV $^{19}F^{+2}$ beam and an average DC beam current (after chopping) of 10 to 15 nA. The target temperture was 145°C and the UHV pressure was below 1×10^{-8} torr.

When a sputtered particle strikes our wheel, it may bounce off rather than be trapped. In order to analyze our experiments we must know the trapping probability. It was measured for uranium atoms sputtered from a metallic target by Libbrecht et al. (1980). They found that for energies below 10 eV approximately 90% of the particles are trapped, while for higher energies, essentially all of them stick. In our case, the sputtered uranium atoms are likely to be bound to one or more fluorine atoms; however, we have assumed that this does not alter the trapping probability. Our neutral spectrum contains only particles with energies less than 10 eV. Because we were measuring only a relative yield and because the trapping probability is uniform in the region below 10 eV, we have not made a correction for it.

After the sputtered material was collected, the wheel was cut into six segments as shown in Weller (1978) Figure 3. Each segment was placed against a piece of mica and the package was exposed to a flux of thermal

neutrons (Gregg 1977). The outline of each segment was scratched into the mica to allow the precise location and orientation of that segment to be reconstructed later. All details of the data analysis technique used here are the same as described in Weller (1978) with the following exception. Weller used a standard least squares analysis to fit points taken along the rim of each segment to a circle. Because of the circular geometry, the equations for the coordinates of the center of the circle were quite complicated and required iterative techniques to solve. In a least squares analysis, one minimizes the quantity

$$\chi^2 = \sum_i (r_i - r)^2$$

with respect to x_o, y_o and r, where x_o and y_o are the coordinates of the center of the "best" circle and r is its radius. Here,

$$r_i = \{(x_i - x_o)^2 + (y_i - y_o)^2\}^{1/2}$$

is the distance of the i^{th} data point at (x_i, y_i) to the center of the circle. The expression for χ^2 contains a sum of terms, each of which involves the unknowns x_o and y_o under a radical. In order to simplify the analysis, it was decided to replace the standard χ^2 with

$$\chi_o^2 = \sum_i (r_i^2 - r^2)^2 \ ,$$

and to minimize this with respect to r^2, x_o and y_o. This yielded simple expressions for x_o and y_o which could be solved exactly. Note that

$$\chi_o^2 \sim \sum_i 4r^2 (r_i - r)^2 \qquad \text{for } r_i \sim r.$$

This is a justified approximation since $r \sim 5$ cm and $r_i - r$ is typically

less than 1×10^{-3} cm. Thus χ_o^2 gives the same expression for $x_o(r)$ and $y_o(r)$ as does χ^2 when $r_i \to r$. The value of r may differ in the two cases; however, it is not an unknown quantity. The calculated value of r is compared against the known value (5.08 cm) as an indication of the accuracy of the analysis scheme. Both methods of analysis gave values of r within 0.05 cm of 5.08 cm consistently. It should be noted that there is no a priori reason that the standard least squares fit should be better than some other similar scheme, it is simply used as a matter of convention. The advantage of using χ_o^2 here is that it reduced the analysis time on a programmable pocket calculator from several hours to a few seconds. Thus coordinates could be calculated as needed during the track counting process. The equations for x_o, y_o and r^2 obtained using χ_o^2 are:

$$x_o = \{(\langle y^2\rangle - \langle y\rangle^2)U - (\langle xy\rangle - \langle x\rangle\langle y\rangle)V\}/2D$$

$$y_o = \{(\langle x^2\rangle - \langle x\rangle^2)V - (\langle xy\rangle - \langle x\rangle\langle y\rangle)U\}/2D$$

$$U = \langle x^3\rangle + \langle xy^2\rangle - \langle x\rangle(\langle x^2\rangle + \langle y^2\rangle)$$

$$V = \langle y^3\rangle + \langle yx^2\rangle - \langle y\rangle(\langle x^2\rangle + \langle y^2\rangle)$$

$$D = (\langle xy\rangle - \langle x\rangle\langle y\rangle)^2 - (\langle x^2\rangle - \langle x\rangle^2)(\langle y^2\rangle - \langle y\rangle^2)$$

$$r^2 = (x_o - \langle x\rangle)^2 + (y_o - \langle y\rangle)^2 + \langle x^2\rangle - \langle x\rangle^2 + \langle y^2\rangle - \langle y\rangle^2 \quad .$$

We have used the standard notation;

$$\langle x\rangle = (1/n)\sum_i x_i \quad ,$$

$$\langle xy\rangle = (1/n)\sum_i x_i y_i \quad , \text{ etc.},$$

where n is the total number of data points measured.

C. RESULTS

In Figure 3 we show the TOF spectrum of uranium sputtered from UF_4 by an 80 keV $^{20}Ne^{+}$ beam. For comparison, in Figure 1 we have reproduced from Griffith (1979), the TOF spectrum of uranium sputtered from UF_4 by a 4.74 MeV $^{19}F^{+2}$ beam. Both runs were performed with no bias voltage on the target and with a single slit 0.45 cm wide. Note that the abscissas of Figures 1 and 3 are the same, i.e. Z=TOF/28 μsec; and the ordinates are arbitrarily normalized in both cases. A striking difference in the two spectra is obvious. Whereas the TOF spectrum in Figure 3 is typical of low energy collision cascade sputtering of both metals and dielectrics (Weller 1978), it is not known whether the spectrum in Figure 1 is typical of high energy sputtering because other targets have not yet been tried. However, there is no a priori reason to expect UF_4 to behave atypically.

Figures 4 and 5 show the data of Figures 1 and 3, respectively, plotted as energy spectra. Figure 4 is taken from Griffith (1979). Collision cascade sputtering theory predicts (Thompson 1968) the energy spectrum of sputtered particles for keV ion bombardment to have the form

$$S(E) \propto E/(E+E_b)^n \quad ,$$

where E_b is the sublimation energy and n is close to three. The curve in Figure 5 corresponds to the equation

$$S(E) \propto E/(E+0.71\ \text{eV})^{2.64} \quad ,$$

while that in Figure 4 corresponds to

$S(E) \propto E/(E+1.2\ eV)^{6.1}$.

Again, high energy sputtering is seen to disagree with predictions for standard collision cascade sputtering.

In Figure 6 we display the TOF spectrum of uranium sputtered from UF_4 by 4.74 MeV $^{19}F^{+2}$, with the charged and neutral particles separated. By sputtered uranium, we mean sputtered particles containing uranium. The method which we use to detect sputtered particles is sensitive only to ^{235}U (Gregg 1977). The region between $2 < t/28\ \mu sec < 16$ contains the charged particles. In the inset we have expanded the region of sharp mass peaks and indicated the expected location of various molecular ions. Each of the molecules is assumed to have a +e charge. The dashed line under the first peak indicates the limiting resolution of our spectrometer due to the finite width of the fixed and rotating slits. A higher resolution spectrum is clearly needed in order to determine the identity and abundance of each molecular species.

A slight deflection of the sputtered ions due to ambient magnetic fields has made the relative peak heights in Figure 6 uncertain to about ± 10%. The ratio of sputtered ions to neutrals inferred from Figure 6 is roughly 20%; however, this should be taken as an upper limit because of electrostatic focusing. Since our detector is only sensitive to individual uranium atoms, the molecules in the second peak are counted twice, the third peak three times, etc. For this reason, the area in the second peak should be divided by two and the third by three in order to obtain the number of clusters in each peak.

The neutral part of the spectrum in Figure 6 is, as expected, quite

similar to Figure 1. It is therefore not expected to be described by collision cascade sputtering theory. In the next section, we present a thermal model of high energy sputtering of dielectrics and suggest a mechanism for attaining thermal equilibrium inside the target which utilizes the ion explosion concept. An explicit expression for the total sputtering yield is calculated and compared with our data.

III. THE MODEL

We now turn our attention to the neutral particles and investigate the possibility that they arise from a thermal mechanism. Perhaps the simplest starting point is to assume that a cylindrical region of constant radius r_o along the incident ion path contains a hot plasma at a temperature T_o (T_o is the kinetic temperature of the atoms, assumed to be in thermal equilibrium). We also assume that the temperature $T=T_o$ is constant from time $t = 0$ to $t = \tau$ and that $T = 0$ for $t>\tau$. The basis for these assumptions will be discussed further in section III. A. The atoms inside this cylinder have a Maxwell-Boltzmann velocity distribution (Reif 1965) given by

$$F(v)dv = n(M/2\pi kT)^{3/2}\ 4\pi v^2\ \exp(-Mv^2/2kT)dv \qquad (2)$$

where v is the magnitude of the velocity, n is the number density of target particles each of which has a mass M, and k is the Boltzmann constant, $k = 8.6 \times 10^{-5}$ eV/^oK. Let the surface of the target have a step potential E_b and consider the particles which cross this surface. If the resultant velocity outside of the target is v' and θ is the angle between $\bar{v}'$ and the normal to the target surface ($v' = |\bar{v}'|$), then the flux of atoms sputtered into solid angle $d\Omega$ at θ with velocity in (v', dv') is (see Appendix A)

$$\Phi(v', \Omega)dv'd\Omega = n(M/2\pi kT)^{3/2}\ \exp(-E_b/kT)\ \exp(-Mv'^2/2kT)\ \cos\theta\ v'^3\ dv'd\Omega\ . \qquad (3)$$

The number of atoms sputtered into our detector at $\theta = 0$ and with solid angle Ω_d with v' in (v', dv') is

$$N(v')dv'\Omega_d = \pi r_o^2 \tau n(M/2\pi kT)^{3/2}\ \exp(-E_b/kT)\ \exp(-Mv'^2/2kT)\ \Omega_d v'^3 dv' \qquad (4)$$

or

$$N(v)dv \propto v^3 \exp(-Mv^2/2kT)dv \qquad (5)$$

where the primes have been dropped in the last expression.

In Figure 7 we show the neutral particle data of Figure 6 plotted as a velocity spectrum with arbitrary normalization. The errors shown arise from counting statistics. A background subtraction has been made as indicated by the dashed line in Figure 6. This line represents the contribution to the spectrum due to very slow particles which wrap around to the beginning of the collector wheel on the next cycle. The line was calculated assuming the data follow the dashed line of Figure 7 at low velocities. The lower solid curve is a two parameter fit with Equation (5). The parameters are the normalization (which is discussed further in section III. B.) and the ratio M/T. A value of 235 amu for M gives T = 3500°K. This solid curve assumes that only single uranium atoms evaporate from the surface. The dashed curve of Figure 7 is a superposition of two curves, each having the form of Equation (5), assuming that 20% of the uranium comes off as U_2 molecules and 80% as U atoms. The temperature in this case is 4100°K and is the same for both species. The purpose of the dashed curve is to show the effect of adding an arbitrary (although reasonable) amount of U_2 to the spectrum. For the sake of simplicity, in further calculations we shall assume that only U atoms are present and that T = 3500°K. The upper solid curve in Figure 7 is the expected velocity spectrum for a non-equilibrium thermal sputtering mechanism which is described in Appendix B.

A. LOCAL THERMAL EQUILIBRIUM

Is it reasonable to expect that atoms near the path of the incident ion reach a condition of local thermodynamic equilibrium (LTE)? When an ion with an energy of approximately 1 MeV/amu enters a solid, virtually all of its energy loss goes to the electrons of the medium. These electrons must give their energy to the lattice atoms more quickly than the energy is thermally conducted away. The most efficient way for electrons to transfer energy to atoms via collisions is for each electron to suffer a head-on elastic collision with an atom each time it travels one lattice spacing. This is, of course, an unrealistic assumption; most of the electron-atom collisions correspond to small angle scattering of the electrons. However, we do in this way establish a lower limit on the time required to transfer the electron's energy into thermal motion. We assume that the recoil electron shares its energy rapidly with other bound electrons until it is degraded to a few eV. At this point the electron can no longer ionize an atom, and transfer of kinetic energy to the atom becomes important. In UF_4, one lattice spacing is d = 4.3 Å; therefore, the time between collisions is $d/v \sim (4.3 \times 10^{-8}/6 \times 10^{7})$ sec $= 7 \times 10^{-16}$ sec where 6×10^{7} cm/sec is the velocity of a 1 eV electron. The fraction of energy transferred to a mass M by a mass m (for $m << M$) in a single head-on elastic collision is $4m/M = 9.3 \times 10^{-6}$ for M = 235 amu and m equal to the mass of an electron. The time for an electron to transfer its energy to a ^{235}U atom is thus:

$$t_{ea} \geq (M/4m)(d/v) = 7.5 \times 10^{-11} \text{ sec.}$$

This time should be shorter than or comparable to the time in which a

significant fraction of the heat is conducted away, t_{hc}. Solving the diffusion equation in a cylindrical geometry with constant thermal conductivity K and heat capacity C we get (Vineyard 1976)

$$T(r, t) = (\varepsilon/4\pi Kt) \exp(-C\rho r^2/4Kt) \qquad (6)$$

For a line source of energy density ε per unit length at $r = 0$ and $t = 0$. T is the temperature and ρ is the target mass density. For $t > C\rho r^2/4K$ the temperature begins to decrease rapidly. Therefore we take

$$t_{hc} = r_o^2/4K,$$

where $K = K/C\rho$ is the thermal diffusivity and r_o is the radius of the thermal spike. For UF_4 at 60^oC, $K = 8 \times 10^{-3}$ cm^2/sec. Using $r_o = 20$ Å (this will be justified in section III. B.), we have

$$t_{hc} = 1.3 \times 10^{-12} \text{ sec.}$$

This is over fifty times smaller than t_{ea}; thus, heating of the lattice through electron-phonon interactions does not appear to be an efficient process in UF_4. Actually the situation is even worse than this. Since the atoms are bound in a lattice, they cannot accept arbitrarily small amounts of energy. The maximum energy which can be transferred to an atom by an electron of a few eV is much smaller than the lowest vibrational energy level of the typical atom in a crystal lattice.

Another, possibly faster, method of heat transfer into the lattice is through "ion explosions". If neighboring lattice atoms are ionized by the passing incident ion and if they are not neutralized too rapidly, they will repel each other, gaining a substantial amount of kinetic energy. If two

adjacent molecules are triply ionized, for example, and recoil from one lattice spacing to three before colliding with other atoms, they will each gain a kinetic energy equal to

$$V = (1/2)(1/d-1/3d)(3e)^2 = 10.2 \text{ eV}$$

When these molecules collide with other stationary molecules, they will transfer approximately one half of their energy per collision. After a few collisions, a condition approaching LTE will be reached if heat is conducted away slowly compared to the collision time. We estimate the collision time, t_{aa}, to be the time for a 1 eV ^{235}U atom to travel one lattice spacing

$$t_{aa} = (4.3 \times 10^{-8}/9 \times 10^{4}) \text{ sec} = 4.8 \times 10^{-13} \text{ sec.}$$

This is several times smaller than t_{hc} and over two orders of magnitude smaller than t_{ea}. The time scales suggest that it may be possible to achieve LTE in a region of radius $\sim r_o$ for a time $\sim r_o^2/4K$.

The fact that t_{hc} and t_{aa} are of the same order of magnitude suggests that the thermal diffusivity may be responsible for quenching sputtering and track registration in certain materials. Sapphire, which has a very high thermal conductivity but a low electrical conductivity, has never been observed to register tracks (Sigrist and Balzer 1977b). Increasing the electrical conductivity could also quench the sputtering or track forming process. This effect has been observed (Fleischer et al. 1975; Robinson and Thompson 1974) and is attributed to mobile electrons which neutralize the ions before they can repel each other.

B. THE SPUTTERING YIELD

From Equation (3), the number of atoms sputtered into solid angle $d\Omega$ at θ with velocity in (v, dv) is

$$S(v, \Omega)dvd\Omega = \Phi(v, \Omega)(\pi r_o^2)(r_o^2/4K)dvd\Omega \ . \qquad (7)$$

Here we assume that the temperature in the spike quickly reaches its equilibrium value and as the cylinder loses heat, its radius contracts while the temperature stays roughly constant. The average spike radius is thus given by r_o. Integrating over solid angle and velocity gives the total sputtering yield,

$$S = \iint S(v, \Omega)dvd\Omega = n(\pi r_o^4/4K)(kT/2\pi M)^{1/2} \exp(-E_b/kT) \ . \qquad (8)$$

We may use this formula with measured values of S, T and E_b in order to deduce a value for r_o. The spike temperature was measured for 4.74 MeV $^{19}F^{+2}$ ions and was found to be 3500°K with M = 235 amu. The same bombarding ions gave a sputtering yield of approximately 5.5 uranium atoms per incident ion (see Figure 8). The binding energy, E_b = 0.71 eV, is obtained from the fit of Equation (1) to the energy spectrum with 80 keV $^{20}Ne^+$ incident on a UF_4 target (see Figure 5). Substituted into Equation (8) these values of S, T and E_b give r_o = 24 Å, which is consistent with the value of r_o used in our calculation of t_{hc} and is also consistent with the observed radii of latent tracks (Fleischer et al. 1975).

The temperature and radius of the spike are expected to depend on the electronic stopping power of the bombarding ion, dE/dx. A related quantity, the primary ionization rate (denoted dJ/dx), has been found by Fleischer et al. (1967) to more accurately describe track registration thresholds. It

is defined as the number of ionizations caused directly by the incident ion per unit path length of the ion. Multiple ionizations are included but secondary ionizations due to scattered electrons are not. A theoretical expression for dJ/dx was presented by Bethe (1930) and for small velocity ($\beta = v/c < 0.1$) reduces to:

$$dJ/dx = Z_e^2(A/\beta^2)\ \ln(B\beta^2), \quad \text{where} \tag{9}$$

$$Z_e = Z\{1-10^{-(1/3)(137\beta/Z^{0.55})}\} \quad . \tag{10}$$

Equation (10) is due to Heckman et al. (1963) with Z the atomic number of the incident ion. The constants A and B in Equation (9) depend on the material through which the ion passes and are difficult to measure or calculate for most solids. For this reason $dJ/dx(\beta)$ is rather uncertain in both magnitude and shape. We have chosen to fix B by fitting data taken from protons and electrons in argon (Schram et al. 1965; De Heer et al. 1966; Griffith 1979), which gives a value of $B = 2.1 \times 10^4$.

In order to obtain an expression relating T and r_o to dJ/dx, we assume (for concreteness) that two ions of charge +N are created each lattice spacing, thus

$$dJ/dx = 2N/d.$$

If E_o is the energy per atom in the spike due to the incident ion, then

$$(3/2)kT = E_o + (3/2)kT_o$$

with T_o the ambient target temperature. Further,

E_o = (kinetic energy per primary recoil)

× (number of primary recoils per lattice spacing)

÷ (number of atoms in the spike per lattice spacing)

$$= \{(1/2)(dJ/dx)^2(de/2)^2(1/d-1/3d)\}\ (2/d)/(n\pi r_o^2)$$

$$= \frac{e^2}{6n\pi r_o^2}\ (dJ/dx)^2 \propto \frac{(dJ/dx)^2}{r_o^2}$$

which gives the desired relation:

$$kT = D\ \frac{(dJ/dx)^2}{r_o^2} + kT_o \qquad (11)$$

where D is a constant.

One further equation relating T, r_o and dJ/dx is needed in order to obtain S in terms of dJ/dx alone. Two cases will be chosen which represent opposite extremes, with the understanding that the true situation lies somewhere between.

Case I: $r_o \propto dJ/dx$

Here, the spike temperature is independent of dJ/dx, and the spike radius expands (contracts) as dJ/dx increases (decreases) to accommodate the changing energy deposition rate. This would occur if the spike temperature were determined only by physical or chemical properties of the target such as melting point, bond strength, etc. In this case we have

$$S \propto (dJ/dx)^4 . \qquad (12a)$$

Case II. r_o = constant

Here, we have the spike radius determined by properties of the target while the spike temperature varies as $(dJ/dx)^2$ for $T_0 << T$. This case appears somewhat less likely and has the disadvantage that the binding energy, E_b, cannot be factored out of the expression for S. In this case we have

$$S \propto (dJ/dx) \exp\{-E_b r_o^2/D(dJ/dx)^2\} \quad . \tag{12b}$$

D is fixed by defining a normalization for dJ/dx and solving Equation (11) for D, using T = 3500°K and the value of dJ/dx at a fluorine energy of 4.74 MeV. Figure 8 shows sputtering yield values as a function of fluorine energy taken from Griffith (1979) along with curves for case I, case II with E_b = 0.5 eV, and dE/dx for comparison. The numbers beside the data points indicate the incident fluorine ion charge state and the error bars correspond to the standard deviations of the measured yields in those cases for which more than one run was performed. Where no error bar is shown, only one run was made.

IV. DISCUSSION

We have emphasized that the dependence of dJ/dx on ion velocity is highly uncertain, being very difficult to calculate or measure for an arbitrary solid. For this reason, a comparison of our model with sputtering yield data for a given ion at different velocities (such as in Figure 8) is of limited value. It would be more useful to compare data for different ions, each having the same velocity. In this case, $dJ/dx \propto Z_e^2$ with $Z_e(Z, \beta)$ empirically determined, as is Equation (10). Since dE/dx also scales as Z_e^2, this method of comparison does not distinguish between dJ/dx and dE/dx. This may be an advantage, however, as it is still a matter of some controversy which quantity (if either) is most relevant to the occurrence of an ion explosion.

In Table I we give sputtering yield predictions for a number of different ions with the same velocity E/M = (1/4) MeV/amu for cases I and II of section III. B. Also shown are measured yields due to Griffith (1979). The calculated values have been normalized to best fit the measured values. The incident charge state of the beam is indicated in the cases where measurements were made; however, it has been shown to have a rather small effect on the total yield (Griffith 1979). Case I is seen to fit the data well except for He^+ for which the measured value is uncertain to about a factor of two. The measured sputtering yields include both high energy sputtering and a small contribution from low energy (collision cascade) sputtering. Since the calculated yields account only for high energy sputtering, when they fall too low, disagreement with the measured values would

be expected. Thus, collision cascade theory predicts a sputtering yield of $\sim 2 \times 10^{-4}$ for He^+ (Griffith 1979), so that the case II predictions are in agreement with the measured value while the case I prediction is not. It should be noted here that although $Z_e(Z, \beta)$ is a more accurately known function than $dJ/dx(\beta)$, several different formulae exist for Z_e and these can differ by as much as 15 for $Z \geq 20$. A 15% difference in Z_e leads to a factor of three difference in the yield calculated for case I. For this reason, sputtering yields for chlorine could not distinguish case I from case II, but yields for lithium or carbon could.

There appears to be some structure in the neutral part of Figure 6, especially at TOF/ 28 μsec = 26 and 44. These "bumps" are roughly two standard deviations outside of a smooth curve through the data. It is difficult to say whether corresponding bumps can be seen in Figure 1, which has worse resolution and statistics than the spectrum in Figure 6. There is a possibility that the structure (which corresponds to energies between 0.45 eV and 1.3 eV) is due to direct recoils from ion explosions occurring at the surface. We will not comment further on this structure here because without more data, we cannot even be sure that it is real.

Although the thermalized ion explosion model presented in this paper describes high energy sputtering of UF_4 quite well thus far, more data are needed to determine if the same model can describe the sputtering of other target materials. Unfortunately, very few data exist at the present time which we feel are applicable to this model. Brown et al. (1978) have measured the sputtering of ice with 1.5 MeV ^4He, ^{12}C and ^{16}O beams and with 1.5 MeV and 0.5 MeV ^1H. We display their results in Table II along with

predictions of our model (case I) which have been normalized to best fit their data (see discussion of absolute yields below). It can be seen that our model fits remarkably well with the ^{4}He, ^{12}C and ^{16}O data but fits the ^{1}H data poorly. We feel this can be understood if one considers the ion explosion mechanism of heat transfer to the lattice. In order for an ion explosion to occur, one would need a minimum of one ionization per lattice spacing. In water, ~30 eV are needed to create one ion-electron pair, so that the minimum dE/dx needed to trigger an ion explosion would be ~ 30 eV per lattice spacing. The maximum dE/dx for the ^{1}H ions used by Brown et al. (1978) was 17.1 eV/(10^{15} molecules/cm^2) ~ 17 eV per lattice spacing. Thus our model would not be expected in its present form to apply to ice sputtering with protons. However, the excitation of higher vibrational modes of the water molecules caused by the proton's passage may drive a similar thermal mechanism even though no ion explosions are taking place.

It would be instructive at this point to estimate the spike radius for heavy ions on ice given the sputtering yields measured by Brown et al. (1978). Using a thermal diffusivity $K = 1.05 \times 10^{-2}$ cm^2/sec for ice at $0^{o}C$ (Fletcher 1970) , a spike temperature of $800^{o}K$ (~3 times the melting point of ice, chosen in comparison with our UF_4 result) and a binding energy $E_b = 0.5$ eV (the sublimation energy of ice) one obtains the following spike radii:

$r_o = 68$ Å for $S = 10$, and

$r_o = 193$ Å for $S = 640$.

These are not unreasonable values given the order of magnitude nature of the

calculation. It thus appears that ice sputtering with heavy ions may also be explained with the thermalized ion explosion model, although more data are needed to confirm this in detail.

The virtue of our model is that concrete predictions can easily be made for comparison with experimental data. In addition to the sputtering yield predictions implied in Tables I and II, one could also look for the effects of thermal diffusivity on high energy sputtering and track registration. For example, in most crystalline dielectric materials, the thermal diffusivity rises very rapidly with decreasing temperature between a few hundred and about ten degrees Kelvin. Thus, a material such as crystalline quartz which registers tracks at room temperature may fail to do so when cooled to a few degrees Kelvin. Some evidence of a dependence of track registration thresholds on thermal conductivity has already been reported (Sigrist and Balzer 1977a,b).

The fact that a fair number of the sputtered particles are charged (probably ~10%) and that a condition of LTE appears to prevail inside the target may have important consequences for secondary ion mass spectroscopy (SIMS). The usual SIMS method of surface analysis (Benninghoven 1973; Werner 1974) produces a mass spectrum of sputtered ions from a solid surface (which may be a metal or dielectric) using Ar or O ions with energies of a few keV. In this energy range, the total sputtering yield is described by Sigmund theory. The method is plagued with several difficulties which limit its usefulness. Sigmund theory is generally applied with a high degree of success only to the sputtering of neutral particles from a clean target containing a single element. No theory presently exists which can

successfully predict ion yields from oxidized metal surfaces and from compounds. In fact, ion yields depend strongly on the degree of surface oxidation, in some cases varying over three orders of magnitude from a clean surface to a fully oxidized one.

Some other problems with SIMS are:

1) During low energy ion bombardment, the beam particles are implanted very near the surface of the target, and this can lead to interference with the ion yield.

2) The resolution of the mass spectrum is limited by the finite width of each mass peak due to the range of initial velocities of the sputtered ions. It is apparent from Figure 5 that a significant number of particles have energies in the range of 10-100 eV.

It may be possible to use high energy sputtering to perform surface analysis of dielectric materials in a manner similar to SIMS. The model described in this thesis applies to the sputtering of compounds as well as single elements if the proper conditions of thermal and electrical conductivity are met. Since we expect the sputtering to occur from a plasma in LTE, the ion yields may be calculable from purely thermodynamic considerations (Andersen and Hinthorne 1973). Also, the problem of ion implantation will be alleviated because the range of our beam particles is greater than a few microns. The line width of the mass peaks is also much smaller with high energy sputtering, as can be seen from Figure 4. The idea of using heavily ionizing particles to desorb ions for mass analysis has already been exploited. For example, Macfarlane and Torgerson (1976b) have used fission fragments to desorb large quasi-molecular ions from organic compounds which are ordinarily difficult to vaporize without decomposition. With subsequent

acceleration and TOF analysis of the ions, they have generated high resolution mass spectra of many non-volatile organic compounds. The line widths of the accelerated ions seem to correspond to a thermal distribution at approximately 60,000°K (Macfarlane and Torgerson 1976a).

A useful experiment which would help to confirm the dependence of the sputtering yield on thermal conductivity is suggested by the work of Ollerhead et al. (1980). Thin UF_4 films of varying thickness (50 Å - 500 Å) could be evaporated onto a good thermal conductor such as copper. The sputtering yield should decrease as the thickness of the UF_4 film decreases because heat is carried away by the conductor. Care would have to be taken that the films were continuous on a microscopic scale. It may be possible to experimentally determine the radius of the hot spike in the following way. Assume (as in case I of section III. B.) that the sputtering yield is proportional to $(dJ/dx)^4$. This implies that $S \propto Z_e^8$, since $dJ/dx \propto Z_e^2$. Now, consider a beam of molecular ions, such as O_2^+, incident on a thin but self-supporting UF_4 film. When a molecule enters the solid, it will be split apart by Coulomb repulsion and multiple scattering. The distance, ℓ, between the two atoms when they exit the film, will be a function of the film thickness. For very thin films, ℓ will be smaller than the spike radius, r_o, and the effective charge of the molecule will be $2Z_e$ where Z_e is the effective charge of each atom. If ℓ is greater than $2r_o$, however, the sputtering yield will be twice that for a single atom of charge Z_e. In the two cases we have

$$S(\ell < r_o) = A(2Z_e)^8 = A\ (2^7)\ (2Z_e^8), \quad \text{and}$$

$$S(\ell > 2r_o) = A\ (2Z_e^8) \quad .$$

Therefore as ℓ goes from less than r_o to greater than $2r_o$ the sputtering yield should decrease by a factor of over 100. If one can calculate the separation ℓ as a function of film thickness and measure the film thickness, then limits can be placed on r_o.

We have presented a model for high energy sputtering of dielectric materials which includes a plausable mechanism for rapid heat transfer to the lattice. Despite its simplicity, this "thermalized ion explosion" model describes the sputtering behavior of UF_4 remarkably well. We feel it is likely that the model can also be used to describe the high energy sputtering of other dielectric materials (such as ice), as well as the phenomenon of track registration.

APPENDIX A

EVAPORATION FROM A HOT SURFACE

Consider a region in the form of a right circular cylinder which contains a "gas" of particles in thermal equilibrium at a temperature T. If the particles interact weakly, their translational degrees of freedom can be treated classically and their distribution function is given by (Reif 1965)

$$f_i(\bar{v}_i)d^3\bar{v}_i = n(M/2\pi kT)^{3/2} \exp(-Mv_i^2/2kT)\, d^3\bar{v}_i \ .$$

where $f_i(\bar{v}_i)d^3\bar{v}_i$ = the mean number of particles per unit volume with center-of-mass velocity in the range between $\bar{v}_i$ and $\bar{v}_i + d\bar{v}_i$.

The subscript i refers to particles which are inside the cylinder and must cross a potential barrier, E_b, at the surface in order to escape. If v_i is the speed of a particle with velocity $\bar{v}_i$, then

$$d^3\bar{v}_i = dv_{ix}dv_{iy}dv_{iz} = v_i^2 dv_i d\Omega_i$$

and $$v_i^2 = v_{ix}^2 + v_{iy}^2 + v_{iz}^2 \ ,$$

so that, in terms of v_i

$$F_i(v_i)dv_i d\Omega_i = n(M/2\pi kT)^{3/2} \exp(-Mv_i^2/2kT)\, v_i^2\, dv_i d\Omega_i \ .$$

Or, changing variables to $E_i = (M/2)v_i^2$,

$$F_i(E_i)dE_i d\Omega_i = n(2E_i)^{1/2}(2\pi kT)^{3/2} \exp(-E_i/kT)\, dE_i d\Omega_i \ .$$

Let $\Phi_i(E_i, \Omega_i)dE_i d\Omega_i$ = the mean flux of particles in (E_i, dE_i) with velocities directed into $d\Omega_i$ which cross a surface whose normal makes an angle θ_i with $\bar{v}_i$.

Then, $\Phi_i(E_i, \Omega_i)dE_i d\Omega_i = F_i(E_i)dE_i(v_i\cos\theta_i)d\Omega_i$

$$= \frac{2E_i n\cos\theta_i}{(M)^{1/2}(2\pi kT)^{3/2}} \exp(-E_i/kT)\, dE_i d\Omega_i \ . \qquad \text{(A1)}$$

Now, let one end face of the cylinder represent the target surface (see Figure 9). Particles which impinge upon this surface will cross if the component of their velocity normal to the surface, $v_i\cos\theta_i$, is greater than $(2E_b/M)^{1/2}$. If $v_i\cos\theta_i$ is less than $(2E_b/M)^{1/2}$, then the particles are specularly reflected. The subscript o refers to the particles outside the cylinder. Referring to Figure 9, we have:

$E_o = E_i - E_b$ and $v_o\sin\theta_o = v_i\sin\theta_i$, which gives

$(M/2)(v_o\cos\theta_o)^2 = (M/2)(v_i\cos\theta_i)^2 - E_b$, and differentiating gives

$v_o^2\cos\theta_o d(\cos\theta_o) = v_i^2\cos\theta_i d(\cos\theta_i)$.

The solid angle, $d\Omega_i = \sin\theta_i d\theta_i d\phi_i$

$$= -d(\cos\theta_i)d\phi_i = -d(\cos\theta_i)d\phi_o \ .$$

Therefore, $\cos\theta_i d\Omega_i = -\cos\theta_i d(\cos\theta_i)d\phi_i = -(v_o/v_i)^2\cos\theta_o d\phi_o d(\cos\theta_o)$.

$$= E_o\cos\theta_o d\Omega_o/(E_o + E_b) \ .$$

Substituting into Equation (A1) for particles outside of the cylinder,

$$\Phi_o(E_o, \Omega_o)dE_o d\Omega_o = \frac{2n}{(M)^{1/2}(2\pi kT)^{3/2}} (E_o + E_b) \exp\{-(E_o + E_b)/kT\}$$

$$\times \frac{E_o \cos\theta_o d\Omega_o dE_o}{(E_o + E_b)} .$$

We will henceforth drop the subscripts and refer only to particles outside of the target:

$$\Phi(E, \Omega)dEd\Omega = \frac{2nE\cos\theta}{(M)^{1/2}(2\pi kT)^{3/2}} \exp\{-(E + E_b)/kT\} dEd\Omega .$$

Finally, in terms of the speed v, we obtain Equation (3) of section III

$$\Phi(v, \Omega)dvd\Omega = n(M/2\pi kT)^{3/2} \exp(-E_b/kT) \exp(-Mv^2/2kT) \cos\theta\, v^3\, dvd\Omega . \qquad (3)$$

This last expression is the flux of particles leaving the target surface with speed in the range between v and v + dv and directed into a solid angle $d\Omega$ at an angle θ with respect to the target surface normal.

APPENDIX B

A NON-EQUILIBRIUM THERMAL SPIKE

In Appendix A we derived an expression for the flux, $\Phi(v,T,\Omega)$, of particles leaving a surface at temperature T with speed in the range between v and v + dv and directed into a solid angle $d\Omega$ at an angle θ with respect to the target surface normal. In general, the temperature of the target surface will be a function of position and time. The velocity distribution of evaporating particles is thus obtained by integrating

$$N(v) = \int_0^\infty 2\pi r dr \int_0^\infty \Phi\{v,T(r,t),\Omega\}dt \quad ,$$

if T(r,t) has cylindrical symmetry. In section III, we chose a particularly simple expression for T(r,t), namely,

$$T(r,t) = T_o \qquad \text{for} \qquad 0 \leq t \leq \tau$$

$$\text{and} \qquad 0 \leq r \leq r_o \quad , \quad \text{and}$$

$$T(r,t) = 0 \qquad \text{otherwise.}$$

This expression for T(r,t) assumes that the evaporation occurs under conditions of thermal equilibrium.

Let us now consider another expression for T(r,t) which represents, in a sense, the opposite extreme. In section III A we presented a solution to the diffusion equation for an instantaneous linear heat source at t = 0 and r = 0:

$$T(r,t) = (\epsilon/4\pi Kt)\ \exp(-C\rho r^2/4Kt) \qquad (6)$$

We used this expression to estimate the thermal conduction time constant, t_{hc}, and used t_{hc} for τ, the duration of the thermal spike. If we now substitute Equation (6) into $\Phi(v,T,\Omega)$ and integrate over r and t, we will obtain another velocity distribution N(v). This non-thermalized distribution should have a broader spread of velocities than the one representing thermal equilibrium and it should fall off much slower at high velocity. The integration can be easily performed using a substitution suggested by Vineyard (1976):

let $\quad t = \varepsilon k\zeta/\{4\pi K(E + E_b)\}$,

and $\quad r = 2(Kt\,\ell n\sigma/C\rho)^{1/2}$.

Then $\quad rdr = 2Kt\,d\sigma/C\rho\sigma \quad$ and $\quad dt = \{\varepsilon k\,d\zeta/4\pi K(E + E_b)\}$. (B1)

This gives, $\quad T(\sigma,\zeta) = (E + E_b)/k\sigma\zeta$. (B2)

From Appendix A,

$$\Phi(v,T) \propto (v^3/T^{3/2})\ \exp(-E/kT)\ \exp(-E_b/kT)$$

for particles which leave the surface directed into solid angle Ω_d at $\theta = 0$. Substituting from Equation (B2) we get,

$$\Phi(v,\zeta,\sigma) \propto \frac{(k\zeta\sigma)^{3/2}\ v^3}{(E + E_b)^{3/2}}\ e^{-\zeta\sigma} \quad ,$$

and, finally, with Equation (B1) we have

$$N(v) \propto \frac{v^3\varepsilon^2 k^{7/2}\ dv}{4\pi K C\rho(E + E_b)^{7/2}} \int_1^\infty \frac{d\sigma}{\sigma^{1/2}} \int_o^\infty \zeta^{5/2}\ e^{-\zeta\sigma}\ d\zeta$$

$$\text{or} \qquad N(v) \propto \frac{v^3\, dv}{\{(Mv^2/2) + E_b\}^{7/2}} \quad . \tag{B3}$$

The upper solid curve in Figure 7 is Equation (B3) with E_b = 0.55 eV and M = 235 amu. The velocity distribution of sputtered particles for any thermal model should lie between the two solid curves, with the upper curve representing conditions farthest from thermal equilibrium and the lower curve representing complete thermal equilibrium. Since our data lie very close to the lower curve, we conclude that conditions approaching LTE prevail during the sputtering process. It is interesting to note that the collision cascade theory of sputtering gives a velocity distribution of the form

$$N(v) \propto \frac{v^3\, dv}{\{(Mv^2/2) + E_b\}^3} \quad .$$

This equation is very similar to Equation (B3) but it falls off slightly slower at high velocities and would, therefore, lie slightly above the upper solid curve in Figure 7. The upper curve of Figure 7 thus represents a region of transition from collision cascade to thermal sputtering.

REFERENCES

Andersen, C. A. and Hinthorne, J. R. 1973, Anal. Chem. 45, 1421.

Benninghoven, A. 1973, Surf. Sci. 35, 427.

Bethe, H. 1930, Ann. Physik 4, 443.

Biersack, J. P. and Santner, E. 1976, Nucl. Instr. Meth. 132, 229.

Brown, W. L., Lanzerotti, L. J., Poate, J. M. and Augustyniak, W. M. 1978, Phys. Rev. Lett. 40, 1027.

Brown, W. L., Augustyniak, W. M., Brody, E., Cooper, B., Lanzerotti, L. J., Ramirez, A., Evatt, R. and Johnson, R. E. 1980, to be published.

Chadderton, L. T., Morgan, D. V., Torrens, I. McC. and Van Vliet, D. 1966, Phil. Mag. 13, 185.

De Heer, F. J., Schutten, J. and Moustafa, H. 1966, Physica 32, 1766.

Dűck, P., Treu, W., Galster, W., Fröhlich, H. and Volt, H. 1980, to be published.

Fleischer, R. L., Price, P. B. and Walker, R. M. 1965, J. Appl. Phys. 36, 3645.

1967, Phys. Rev. 156, 353.

1975, Nuclear Tracks in Solids (University of California Press, Berkeley).

Fletcher, N. H. 1970, The Chemical Physics of Ice (Cambridge University Press).

Gregg, R. 1977, Ph.D. Thesis, California Institute of Technology.

Gregg, R., Switkowski, Z. E. and Tombrello, T. A. 1977, Nucl. Instr. Meth. 144, 613.

Gregg, R. and Tombrello, T. A. 1978, Rad. Eff. 35, 243.

Griffith, J. E. 1979, Ph.D. Thesis, California Institute of Technology.

Griffith, J. E., Weller, R. A., Seiberling, L. E. and Tombrello, T. A. 1980, Rad. Eff., in press.

Haff, P. K. 1976, Appl. Phys. Lett. 29, 473.

Heckman, H. H., Hubbard, E. L. and Simon, W. G. 1963, Phys. Rev. 129, 1240.

Libbrecht, K. G., Griffith, J. E., Weller, R. A. and Tombrello, T. A. 1980, Rad. Eff., in press.

Macfarlane, R. D. and Torgerson, D. F. 1976a, Phys. Rev. Lett. 36, 486. 1976b, Inst. J. Mass Spectrom. Ion Phys. 21, 81.

Ollerhead, R. W., Bøttiger, J., Davies, J. A., L'Ecuyer, J., Haugen, H. K. and Matsunami, N. 1980, to be published.

Reif, R. 1965, Fundamentals of Statistical and Thermal Physics (McGraw-Hill Book Co.).

Robinson, J. E. and Thompson, D. A. 1974, Phys. Rev. Lett. 33, 1569.

Schram, B. L., De Heer, F. J., Van der Weil, M. J. and Kistemaker, J. 1965, Physica 31, 94.

Sigmund, P. 1969, Phys. Rev. 184, 383.

Sigrist, A. and Balzer, R. 1977a, Helv. Phys. Acta 50, 49. 1977b, Rad. Eff. 34, 75.

Thompson, M. W. 1968, Phil. Mag. 18, 377.

Vineyard, G. H. 1976, Rad. Eff. 29, 245.

Weller, R. A. and Tombrello, T. A. 1978, Rad. Eff. 37, 83.

Weller, R. A. 1978, Ph.D. Thesis, California Institute of Technology.

Werner, H. W. 1974, Vacuum 24, 493.

Table I

Uranium sputtering yield predictions for ten different beams incident at (1/4) MeV/amu on UF_4. The conditions implied by Case I and Case II are described in section III. B. Measured uranium sputtering yields from UF_4 that are taken from Griffith (1979) are given in the last column (see section IV.).

Table I

Beam	Z_e	S(U atoms/ion) Case I	Case II E_b = 0.5 eV	Case II E_b = 0.7 eV	measured
H	0.91	1.5×10^{-5}			
$^4He^+$	1.62	1.5×10^{-3}			$\sim 2 \times 10^{-4}$
Li	2.21	1.7×10^{-2}	1.2×10^{-15}	1.2×10^{-21}	
C	3.59	0.83	0.13	3.4×10^{-2}	
$^{16}O^{+2}$	4.32	3.7	3.0	2.3	3.9 ± 1
$^{19}F^{+2}$	4.66	6.7	6.7	6.7	5.6 ± 1
$^{20}Ne^{+2}$	4.97	11.3	11.6	13.7	11.7 ± 2
S	6.59	108	54	93.5	
Cl	6.83	143	61	110	
Ar	7.06	187	69	125	

Table II

Measured H_2O sputtering yields taken from Brown et al. (1978), shown with the electronic stopping power of each beam used. In the last column are yields predicted by our model (Case I) normalized to best fit the data (see section IV.).

Table II

Beam	dE/dx (10^{-15} eV cm^2 per molecule)	S (molecules per ion)	$(4 \times 10^{-4}) \times (dE/dx)^4$
^{1}H	6.8	0.2 ± 0.04	8.6×10^{-4}
^{1}H	17.1	0.4 ± 0.08	0.034
^{4}He	71	10 ± 2	10.2
^{12}C	189	520 ± 100	510
^{16}O	201	640 ± 130	653

Figure 1

The TOF spectrum of particles containing uranium sputtered from UF_4 by 4.74 MeV $^{19}F^{+2}$, reprinted from Griffith (1979). The wheel for this run had one slit measuring 1.11 cm by 0.45 cm and there was no bias voltage on the target (see section I.). The yield is in arbitrary units and Z = TOF/28 μsec.

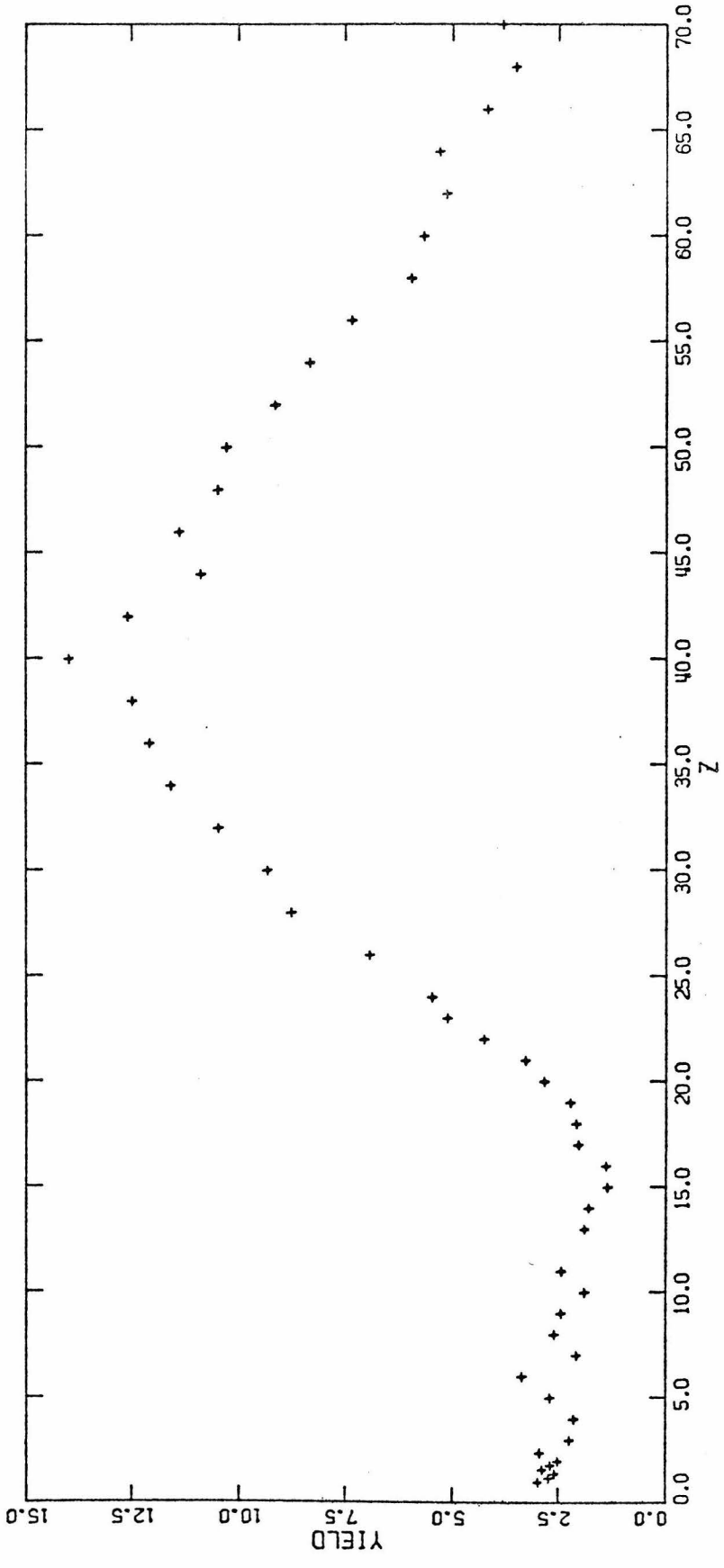
YIELD
0.0
2.5
5.0
7.5
10.0
12.5
15.0
Z
0.0
5.0
10.0
15.0
20.0
25.0
30.0
35.0
40.0
45.0
50.0
55.0
60.0
65.0
70.0

Figure 1

Figure 2

A schematic drawing of the experimental apparatus used to determine the TOF spectra (see section II. A.).

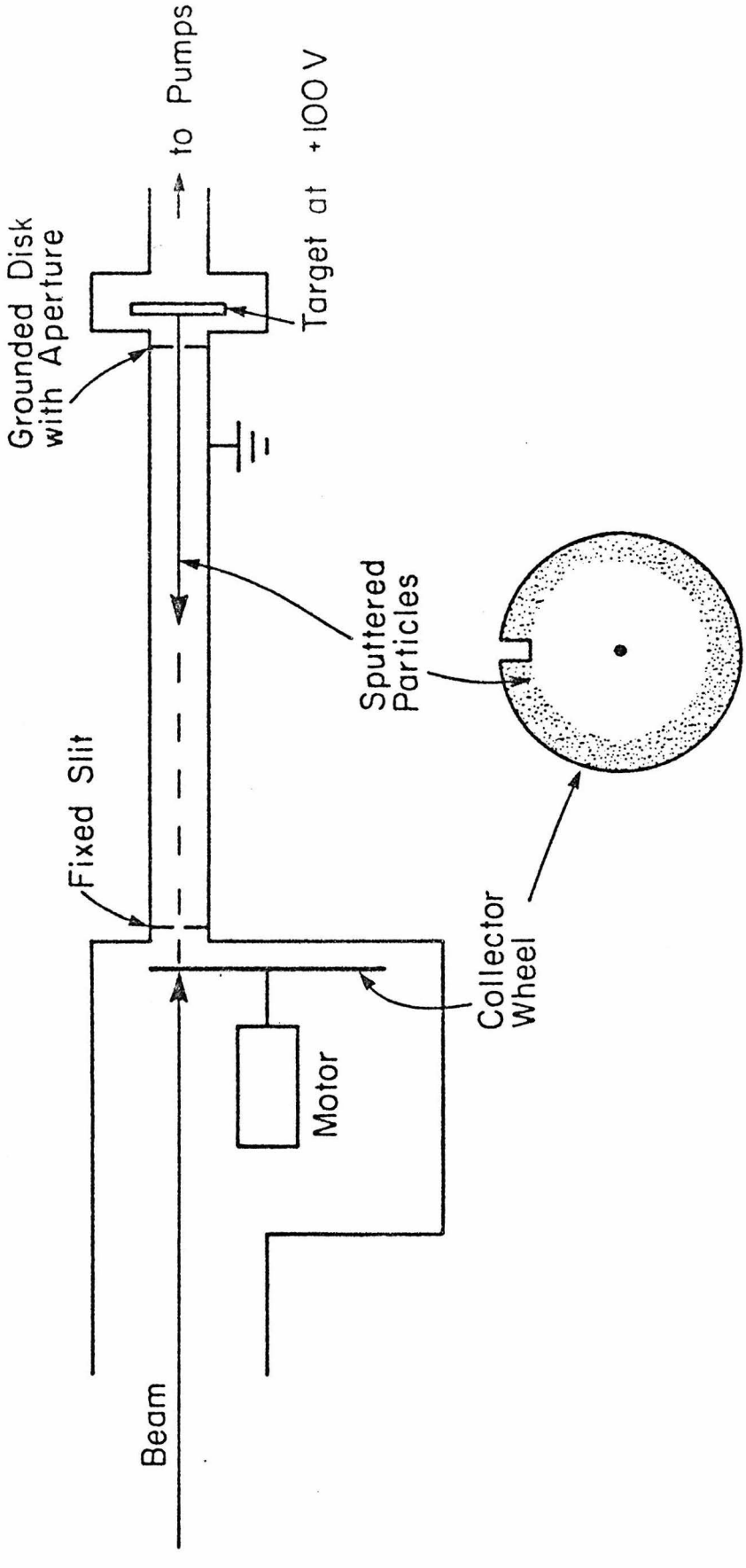
to Pumps
Target at +100 V
Grounded Disk with Aperture
Sputtered Particles
Fixed Slit
Collector Wheel
Motor
Beam

Figure 2

Figure 3

The TOF spectrum of particles containing uranium sputtered from UF_4 by an 80 keV $^{20}Ne^+$ beam. The wheel for this run had one slit measuring 1.11 cm by 0.45 cm and there was no bias voltage on the target (see section II. B.).

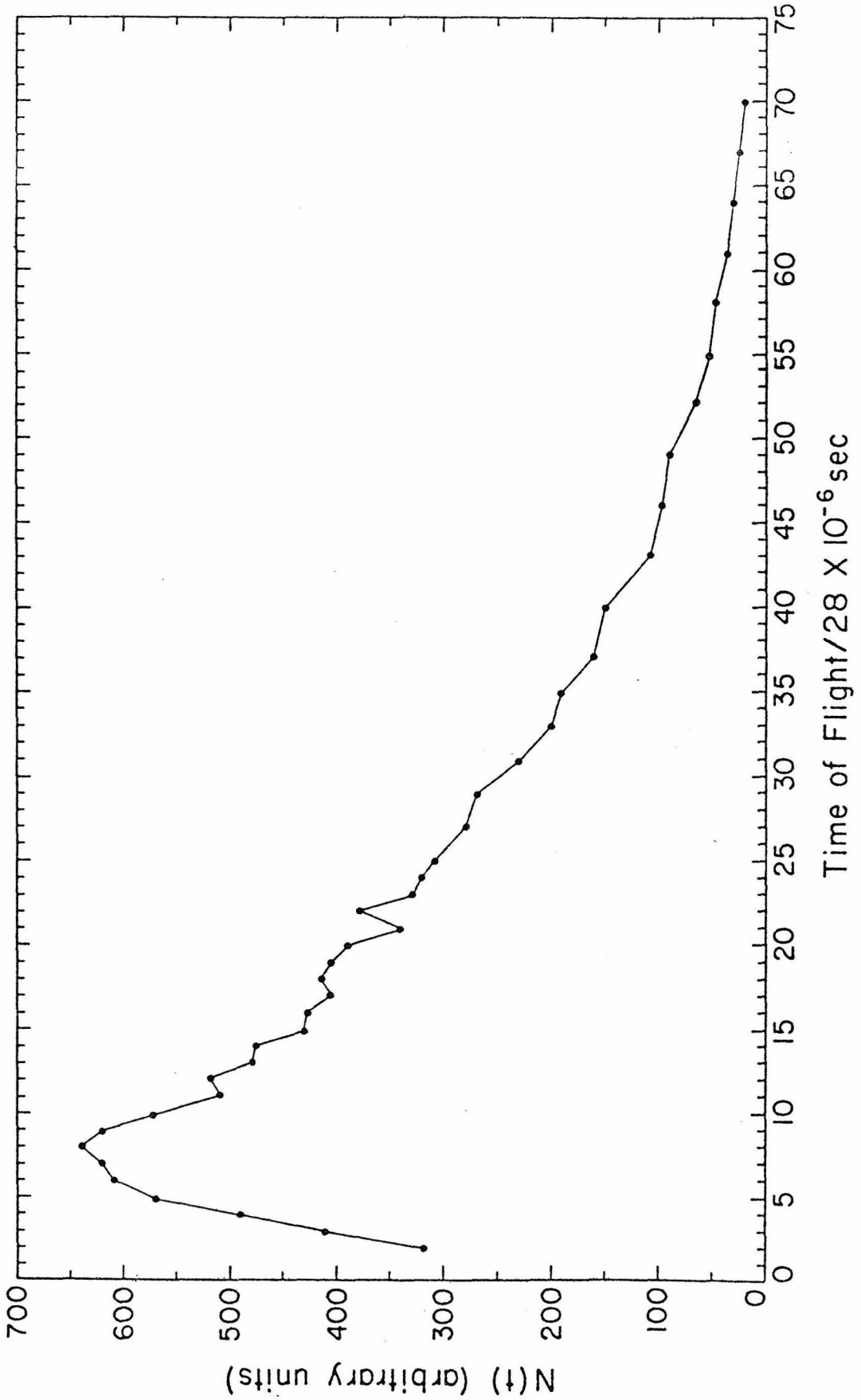
N(t) (arbitrary units)
0
100
200
300
400
500
600
700
0
5
10
15
20
25
30
35
40
45
50
55
60
65
70
75
Time of Flight/28 X 10⁻⁶ sec

Figure 3

Figure 4

This figure shows the data of Figure 1 plotted as an energy spectrum with arbitrary normalization, reprinted from Griffith (1979). The curve is a fit to the formula

$$S(E) \propto E/(E + 1.2\ eV)^{6.1}$$

(see section II. C.).

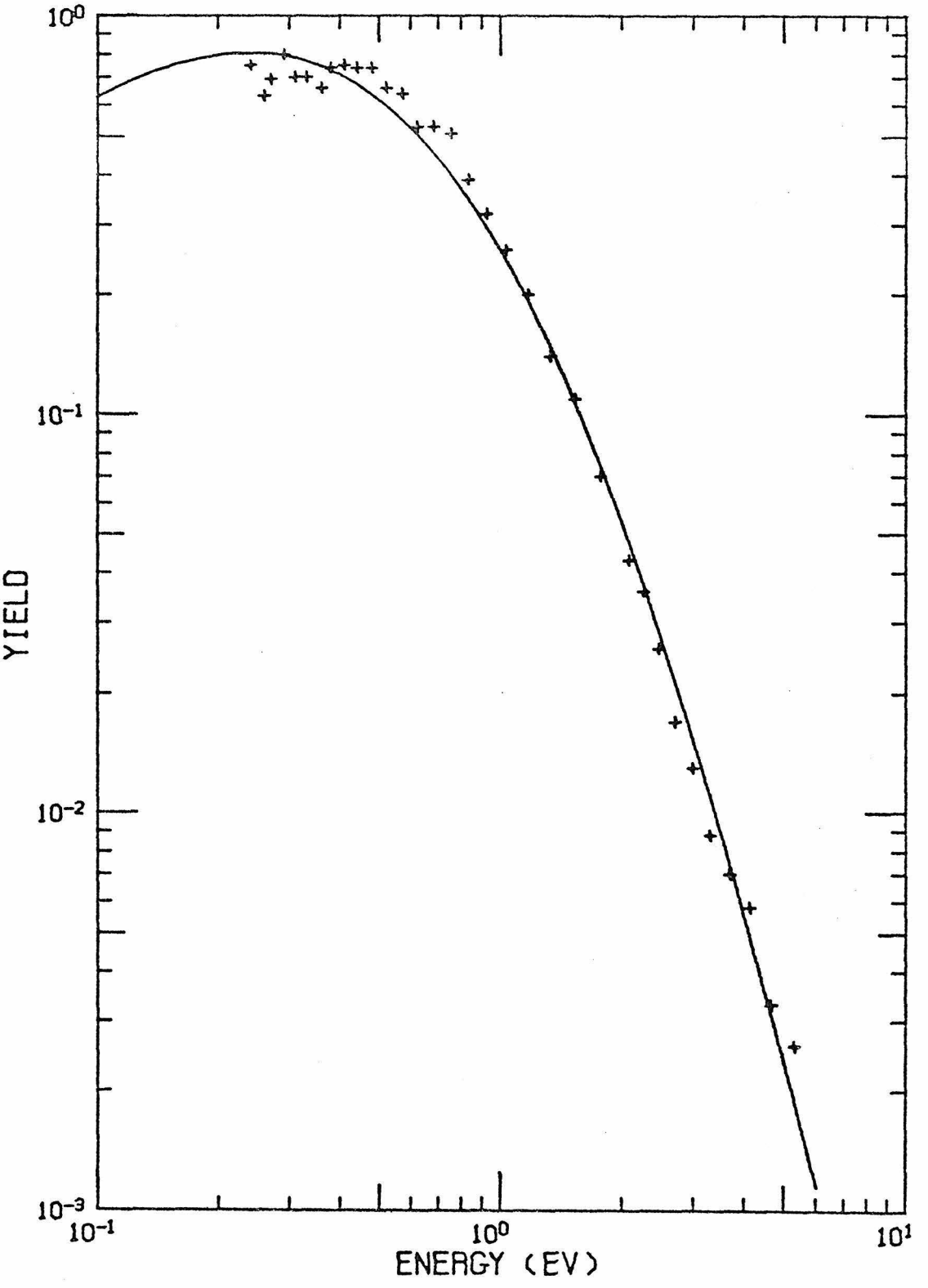

Figure 4

Figure 5

This figure shows the data of Figure 3 plotted as an energy spectrum with arbitrary normalization. The curve is a fit to the formula

$$S(E) \propto E/(E + 0.71 \text{ eV})^{2.64}$$

(see section II. C.).

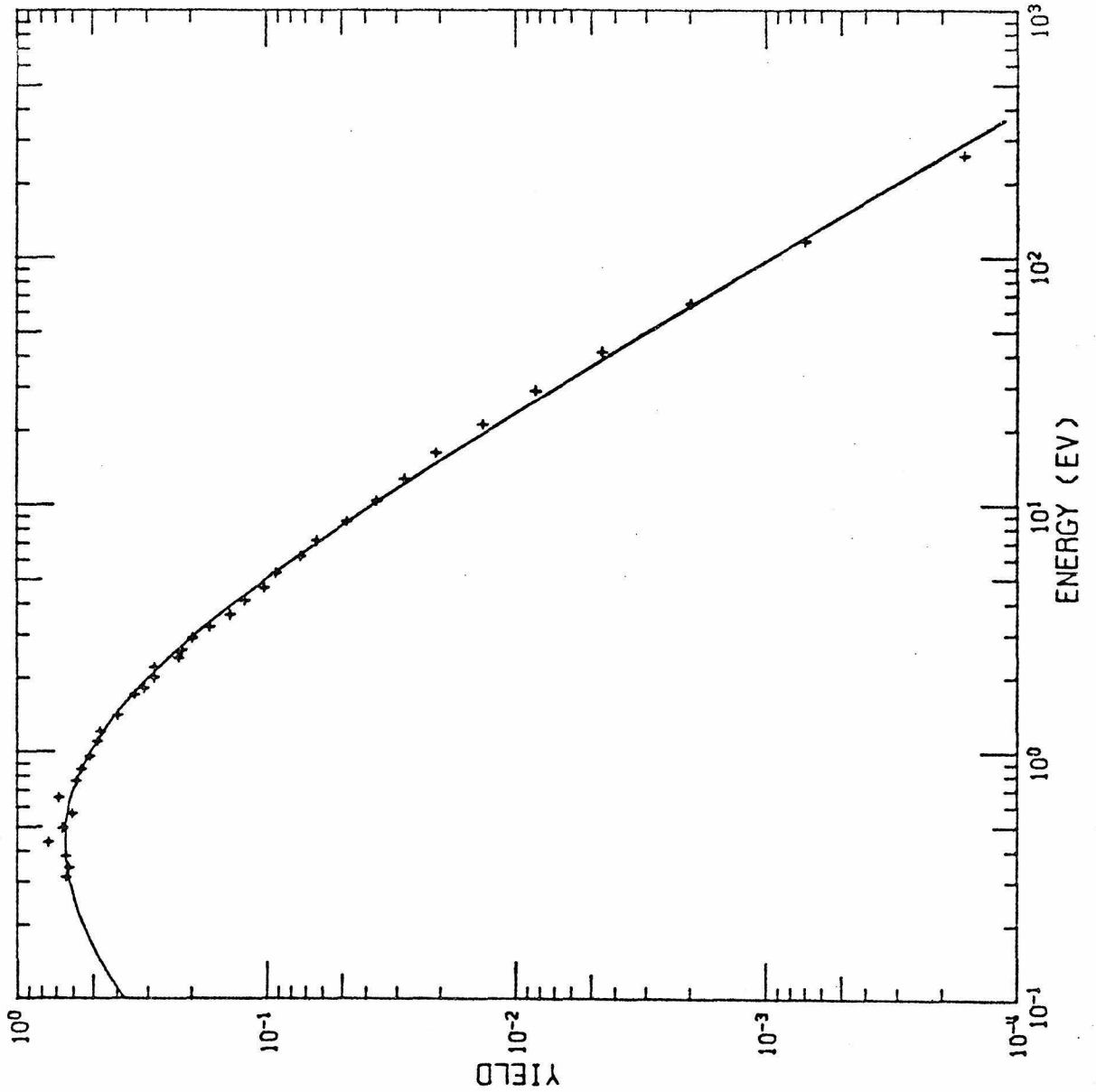

Figure 5

Figure 6

The TOF spectrum of particles sputtered from a UF_4 target with 4.74 MeV $^{19}F^{+2}$. The sputtered ions were accelerated through +100 volts and lie in the region TOF/28 μsec < 16. The sharp peaks at low TOF are displayed in expanded form in the inset, and the expected positions of various singly charged molecular ions are shown. The uncertainty in position of the molecular ions shown is approximately $\pm$ 20 amu. The dashed line under the first peak indicates the limiting resolution of the spectrometer, and the dashed line below the TOF spectrum represents the slow neutral particles which wrap around the wheel a second time (see section II. C.).

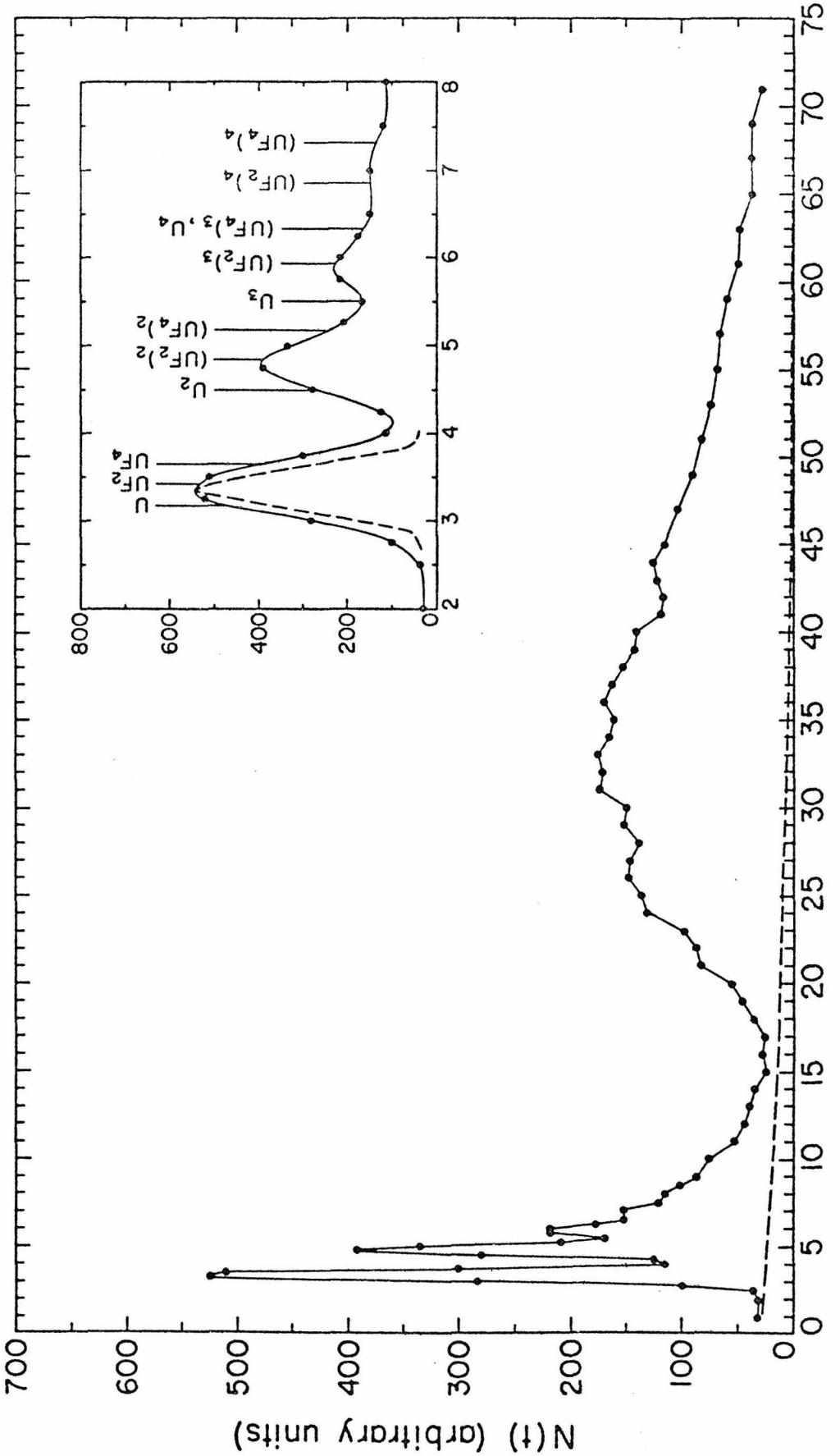
N(t) (arbitrary units)
Time of Flight/28 X 10⁻⁶ sec
U
UF4,2
U2
(UF2)2
(UF4)2
U3
(UF2)3
(UF4)3,U4
(UF2)4
(UF4)4

Figure 6

Figure 7

The velocity spectrum of neutral uranium sputtered from a UF_4 target with 4.74 MeV $^{19}F^{+2}$. The error bars represent counting statistics. The lower solid curve is Equation (5) with M = 235 and T = 3500°K, with the normalization chosen to best fit the data. The dashed curve is a superposition of two curves, each having the form of Equation (5), assuming 20% of the uranium comes off as U_2 molecules and 80% as U atoms. Both species are assumed to be at T = 4100°K (see section III.). The upper solid curve is Equation (B3) with E_b = 0.55 eV and M = 235 amu (see Appendix B).

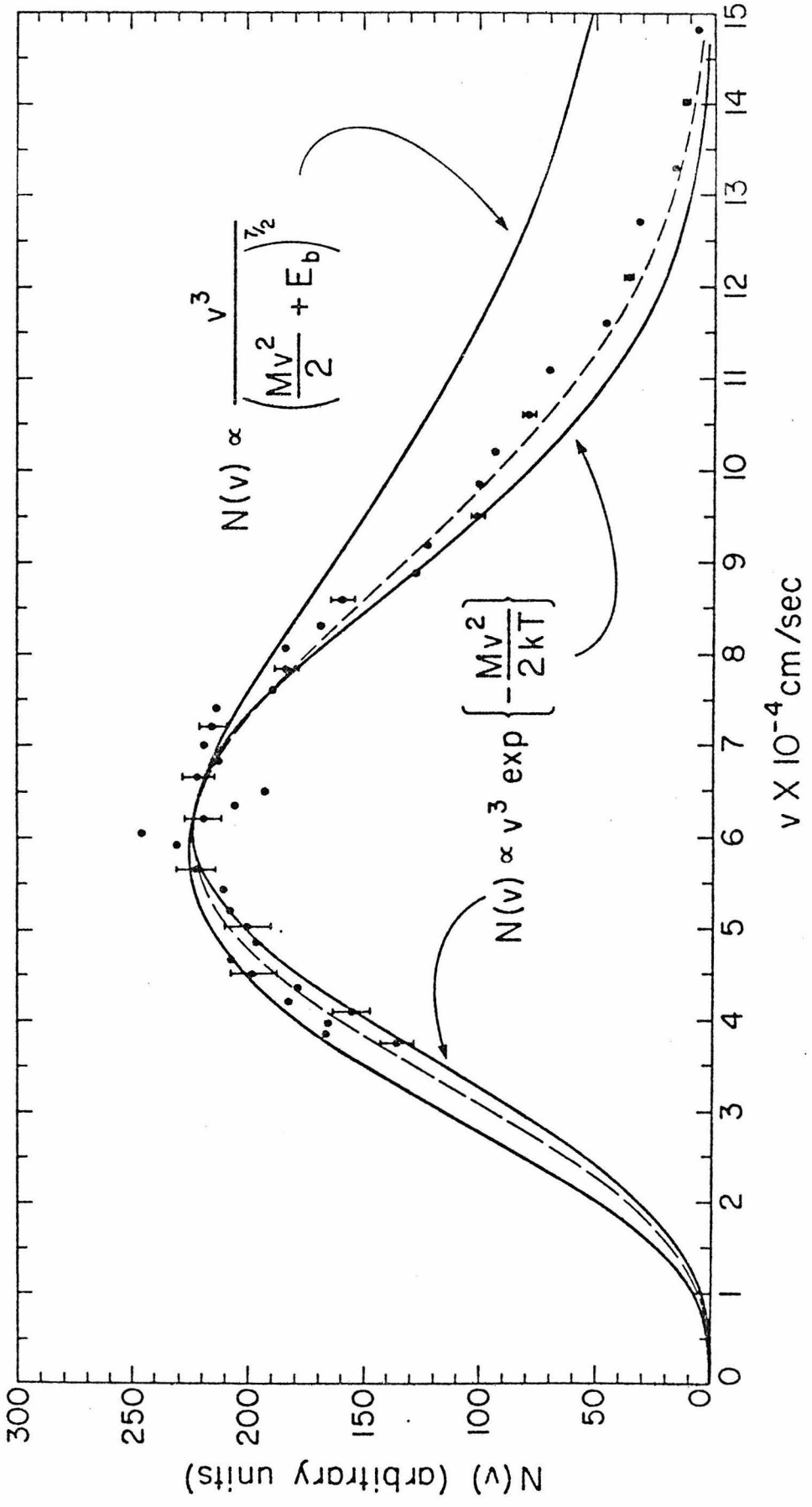
N(v) (arbitrary units)
v X 10^-4 cm/sec
N(v) ∝ v^3 exp {-Mv^2/2kT}
N(v) ∝ v^3 / (Mv^2/2 + E_b)^7/2

Figure 7

Figure 8

The sputtering yield values as a function of fluorine energy. The numbers beside the data points indicate the incident fluorine charge state and the error bars correspond to the standard deviations of the measured yields in those cases for which more than one run was performed. The dash-dot curve is dE/dx with the maximum corresponding to ~ 300 eV/Å. The solid and dashed curves are Equations (12a) and (12b), respectively, and are normalized to best fit the data (see section III. B.). Part of this figure is taken from Griffith (1979).

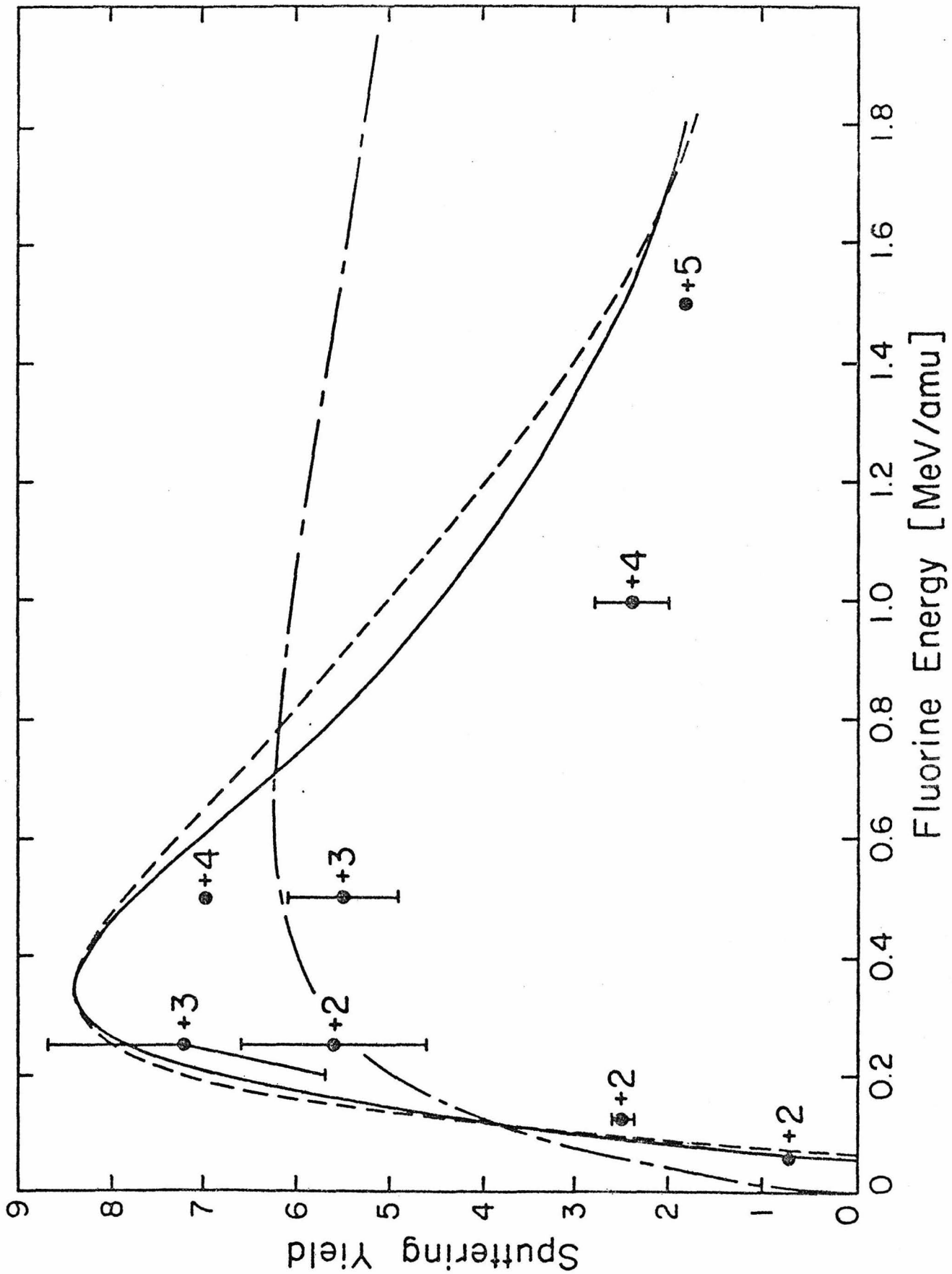
Sputtering Yield
Fluorine Energy [MeV/amu]
0
1
2
3
4
5
6
7
8
9
0
0.2
0.4
0.6
0.8
1.0
1.2
1.4
1.6
1.8
+2
+2
+2
+3
+3
+4
+4
+5

Figure 8

Figure 9

This is a schematic drawing of the refraction of a target particle as it is evaporated from a hot surface. The particle has a velocity $\bar{v}_i$ just inside the surface and a velocity $\bar{v}_o$ just outside. There is a potential step of height E_b at the target surface (see Appendix).

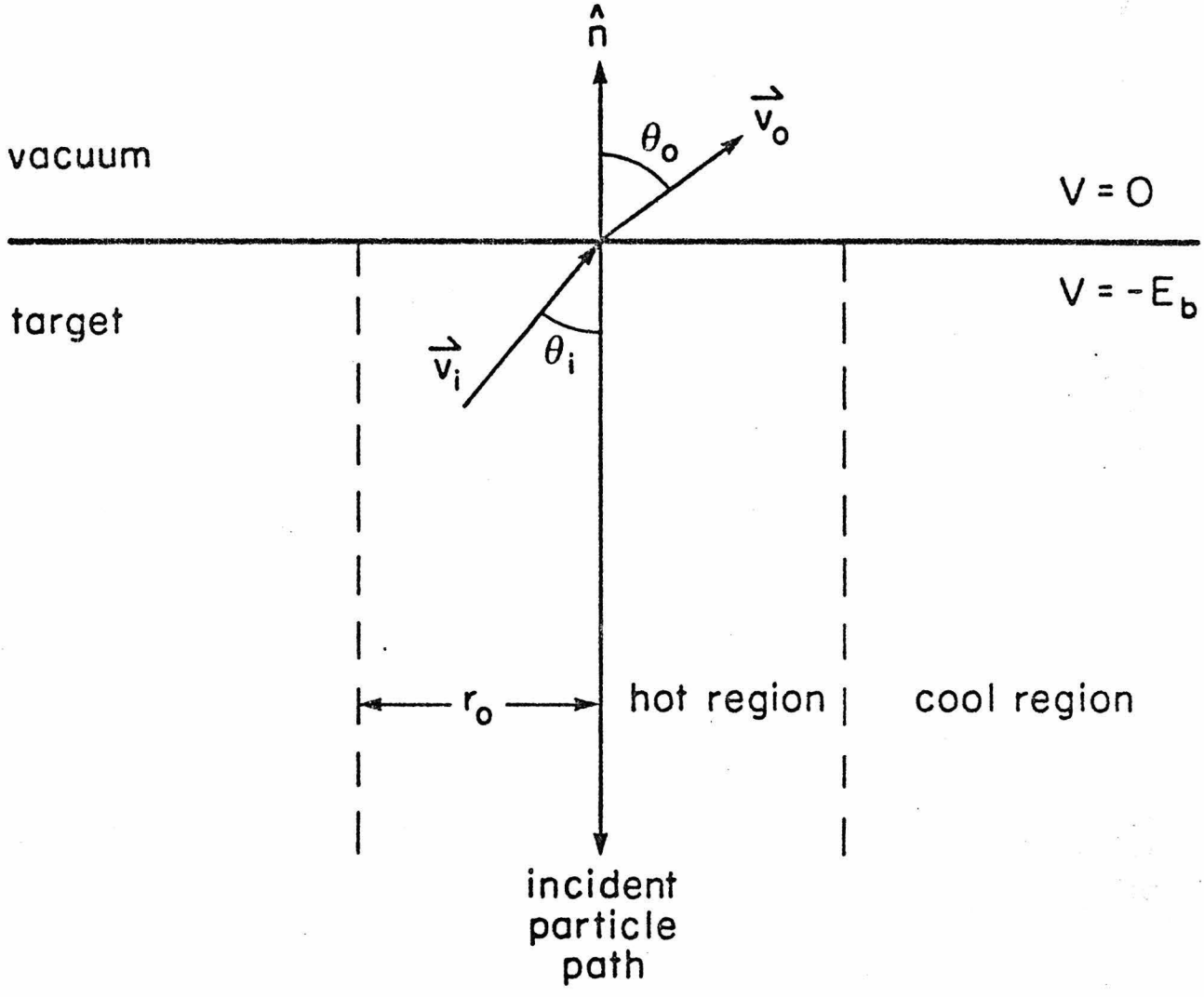
$\hat{n}$
$\vec{v}_o$
θ_o
vacuum
V = 0
target
V = -E_b
$\vec{v}_i$
θ_i
r_o
hot region
cool region
incident
particle
path

Figure 9